Proceedings World Geothermal Congress 2020+1
Reykjavik, Iceland, April - October 2021

Modelling of the Non-Condensable Gases Reinjection for Geothermal Emission Control (GECO Project)

Vlasios Leontidis[1], Martin Gainville[1], Laurent Jeannin[2], Marc Perreaux[2] and Christine Souque[1]

[1] IFP Energies Nouvelles, 1 & 4 avenue de Bois Préau, 92852 Rueil-Malmaison, France

[2] Storengy SAS, 12 rue Raoul Nordling, 92274 Bois-Colombes cedex, France

vlasios.leontidis@ifpen.fr

Keywords: re-injection well, non-condensable gases, CO2 storage, two-phase modelling

ABSTRACT

High enthalpy geothermal systems, including vapour-dominated reservoirs, may contain non-condensable gases (NCGs). Thus, the steam production is accompanied with emissions of geothermal gases (CO_2, H_2S, H_2….) initially dissolved in the liquid phase or mixed in a vapour phase at depth in the reservoir. In order to reduce the environmental impact of geothermal exploitation resources and avoid emission of greenhouse or toxic gases in the atmosphere, NCGs have to be captured and re-injected. This approach leads to an environmentally friendly exploitation, pressure support and geothermal resource sustainability. For low NCG content, the gases can be fully dissolved at the surface in the condensed water and re-injected. However, for high concentration of NCG, the dissolution is only partial and a two-phase flow (gaseous NCGs and condensed water) needs to be re-injected. We focus here on presenting the fluid flow model of a completion configuration ensuring the simultaneous re-injection of NCGs and condensed water in the same well. A specific geothermal site was selected as base case, main characteristics of which are the high concentration of NCGs on the production geothermal fluid (mainly vapour) and the low injection reservoir pressure. The objective of the current work is to study the complete operation of reinjection under non-isothermal steady state conditions and to demonstrate its efficiency. The prototype well completion consists in an annulus completion with water circulating in one part and non-condensable gases in the other. The two fluids are mixed at a given depth and through several injection points. A part of the non-condensable gases is then progressively dissolved into the liquid phase within the flow and the mixture flow is re-injected into the reservoir at the bottom hole. The recompression occurring in the two-phase flow section of the well allows reduction of NCG compression at the surface improving the overall efficiency and the cost of the system. The model takes into account the single phase flows of water and NCGs, the hydrodynamics of the two-phase downward flow with two major components (H_2O and CO_2) in the injected fluid, constitutive laws for the mixtures, the dissolution of gas into water, and the evaporation of the aqueous phase into the gaseous phase. Finally, the heat exchange between the surrounding ground, the annulus and the central part of the well is modelled.

1. INTRODUCTION

Geothermal fluids may have relatively high content of non-condensable gases (NCGs), including Green House Gases such as methane (CH_4) and carbon dioxide (CO_2) and highly toxic gases such as hydrogen sulphide (H_2S). Geothermal fluids extracted from the subsurface including NCG have usually to be treated before venting in the atmosphere. The GECO (Geothermal Emissions Control) European project focuses on cost-effective non-carbon emitting geothermal energy solutions across Europe and the World. One possible way is to ensure the total reinjection of the geothermal fluids, NCGs together with the condensed water in injection wells, in order to minimize the environmental impact.

Injection processes are also performed for CO_2 capture and storage (Carbon Capture and Sequestration, CCS) in underground geological formations, such as depleted oil and gas reservoirs and deep saline aquifers. The typical method to inject CO_2 into these subsurface rock formations is as a single CO_2 phase, gaseous or supercritical. Once injected, carbon storage proceeds through a sequence of four trapping mechanisms: structural trapping, residual trapping, solubility trapping, and mineral trapping (Benson and Cole, 2008). The simultaneously co-injection of CO_2 and water/brine in saline aquifers is also a technique used for CCS (Burton and Bryant, 2009; Eke et al., 2009; Koide and Xue, 2009; Rathnaweer et al., 2016; Shariatipour et al., 2016; Suzuki et al., 2013; Zendehboudi et al, 2011; Zendehboudi et al, 2013; Zirrahi et al, 2013). Shafaei et al. (2012) proposed a “reverse gas-lift” technology in which water is pumped into the well through a tube and CO_2 is injected simultaneously using the annulus space between the tubing and the well casing. Several one way gas-lift valves are installed on the tube string providing communication between the annulus and the central tubing. A numerical model was developed and it was shown that, compared to the conventional technique of CO_2 injection, the technique offers lower cost of well head CO_2 compression.

The thermodynamic, the dissolution kinetics and the hydraulic conditions are key-parameters to secure the NCGs and condensed water reinjection processes. The complete dissolution of NGCs on water depends on pressure and temperature conditions and the relative amount of water. For example, 2.2 %w of CO_2 can be dissolved in pure water at 50 bar and 90 °C and the double of this amount at 65 °C (Duan and Sun, 2003). For high concentration of NCGs the compression requirements would be enormous for achieving a single liquid phase mixture at the surface. A practical and economical solution could be the reinjection under two-phase flow. However, in that case, the completion of the well should be carefully designed.

Over the last decade, a process (CarbFix) for capturing and injecting CO_2 and other acid gases into the subsurface where they are stored as stable minerals, has been developed and installed in Iceland on existing geothermal power plants. The original CarbFix approach was to co-inject water and soluble gases into the subsurface. Gas was released as fine bubbles into the water at depth, which completely dissolved into the water before it entered the porous aquifer rocks. In this case, water was pumped in the annulus space and gas was injected in the central tubing (Sigfusson et al., 2015). To reduce costs and to streamline the original CarbFix approach, CO_2 and H_2S dominated gas mixture was and continues to be directly captured from the power plant exhaust gas stream

by its dissolution into pure water in a scrubbing tower (Aradotti et al., 2015). This water interacted with the exhaust gas stream dissolving the water-soluble gases. The pressurized gas-charged water was transported to the injection well, where it was injected together with additional effluent water into the subsurface at certain depth.

A commercial multiphase flow simulator has been used for modelling the reinjection well of NCGs and water for a geothermal site to be installed in Italy (Stacey et al., 2016). The completion design was similar to the CarbFix technology (water to annulus space and gas to the central tube) and sensitivity studies were performed to define the optimal mixing depth and the inlet conditions (gas compression and water pumping requirements). They found out that the reinjection depth for minimizing the injection pressure and thus the cost is around 300-500 m below the surface.

For the reinjection process of this study, a double annular completion with water circulating in the tubing and NCGs in the annular has been selected. The two fluids are mixed at a certain depth and a part of the NCGs is then progressively dissolved into the water flow and the mixture is re-injected into the reservoir at the bottom hole. The prototype completion extends the original CarbFix solution (Sigfusson et al., 2015) to the case of high NCG content and is similar to the solution proposed by Shafaei et al. (2012) for CO_2 storage in aquifers. Recompression of the gas occurs in the two-phase flow section of the well and allows reduction of NCG compression at the surface: this approach improves the overall efficiency and the cost of the system. A 1D model was developed to simulate the reinjection approach and to describe the non-isothermal steady state two-phase (water and NCGs) downward vertical flow from the injection wellhead down to the bottom hole. Downward vertical two-phase flows have been far less investigated compared to upward flow; these flows have a specific complexity related to gas entrainment at low flow rates which has to be carefully studied for the combined reinjection process.

The proposed design and the developed model was applied for a specific geothermal site located on the Tuscany area, North of Italy (a site of the GECO project), where a zero emission power plant will be developed. The operating concept is a “closed loop”, which requires the total reinjection of the condensate steam and the high concentration of NCGs to a low pressure (depleted) reservoir. The completion design proposed in this study is not case-specific and can be applied to other geothermal sites.

2. SYSTEM DESCRIPTION

The well completion considered is made up of a tubing and a casing (Fig. 1). Along the inner tubing several points of injection (using valves) are installed to connect the annular space and the tubing. Water is injected in the tubing, while gas in the annular space flows through valves and is mixed at depth with water in the tubing. Depending on the reservoir injectivity and the initial reservoir pressure that may be largely lower than the hydrostatic pressure for geothermal steam reservoirs, such as in Italy, the water column may not reach the wellhead, when water is injected at constant flow rate. In that case, a “free fall” section is present at the top part of the central tubing. To allow gas injection in the water phase, at least one open injection valve has to be located below the water level. The use of multiple injection points provides flexibility to operate in different situations, to facilitate the start-up operations and to secure the gas entrainment with the gas-liquid downward flow.

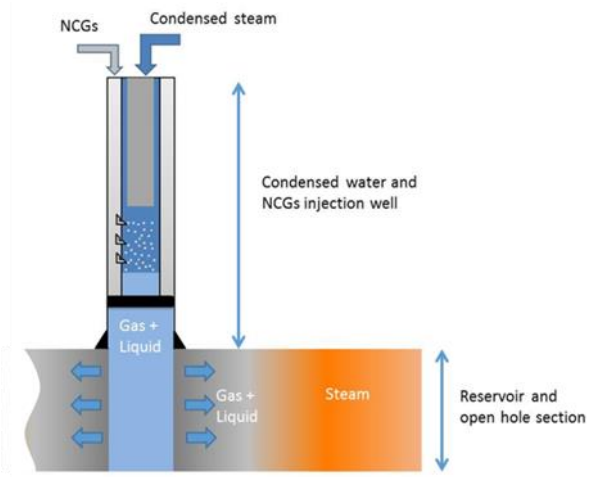

Figure 1: Well completion.

At the surface, the system consists of the gas compression and the water pump stations, for the NGCs and water streams respectively. The water results either from the condensation of the geothermal fluid in flash separators (single or multiple) before the power generation or from a binary cycle (Organic Rankin cycle) where the heat of the geothermal fluid is used to vaporise (flash) a secondary fluid which then drives the turbines (DiPippo, 2016). The injection of the two fluids in the wellhead takes place separately and the mixing occurs deeper in the well.

To secure the injection of the gas to the central tubing through the valves and to avoid backflow of liquid in the annulus part, the opening of injection point is determined by the following rules: on one hand, the fluid pressure in the central tubing has to be lower than the gas pressure in the annular space, at the injection point considered; on the other hand, the liquid pressure in the central tubing has to be greater than a certain pre-defined pressure threshold. Indeed, this threshold ensures that the level of the liquid column is above the injection point.

This approach is particularly advantageous as it provides effective recompression of the gas thanks to the gas liquid mixture column in the tubing, thereby limiting the gas injection pressure at the wellhead. Moreover, injecting the gas into a stable liquid column

makes it possible to promote mixing and two-phase flow. Finally, the multipoint injection solution facilitates start-up operations by limiting gas compression at the wellhead.

3. MODEL DESCRIPTION

A steady state 1D non-isothermal multicomponent and two-phase flow model of the process described above was developed considering the transfer of mass, heat and momentum. More detailed, the model takes into account the single phase flows of liquid and gas, the hydrodynamics of the two-phase downward flow, constitutive laws for the mixtures, the dissolution of CO_2 into water, the evaporation of the aqueous phase into the gaseous phase, the flow of the fluid through the injection orifices/valves, and finally the heat exchange between the well completion and the surrounding formulation.

3.1 Hydrodynamic modelling

The hydrodynamic modelling consists in calculating the velocities of the fluids and the pressure drop along the flow. For single phase flows, the calculations are quite simple and well established. However for two-phase downward flows, the calculations are more complicated and additional flow parameters, such as the void fraction (or liquid hold-up) and the phase distribution (flow regime), must be defined. For example in downward two-phase flows, the pressure drop depends strongly on the way the phases are organized inside the control volume.

Even though that two-phase gas-liquid flow attracted much attention over the last several decades, mainly for oil & gas applications, vertical downward flow was rarely considered and there is a lack of extensive experiments and data. Most of the available data and models are coming from research done for the nuclear industry and the number of studies dealing with fluids different than water and air, at high operational pressure and for relative large diameters (above 3 in) remains limited.

3.1.1 Flow Regime Identification

Initially, at the start-up of the reinjection, only liquid is injected from the well head at the central tubing. Depending on the reservoir injectivity and pressure, the level of water raises until a specific depth. In the proposed injection solution, gas is always injected from the annulus to the tubing space below the water free surface. Different flow regimes may be observed depending on the local conditions and the valve position in the tubing.

Single phase gas flow (denoted *G*) occurs in the annulus. Single phase liquid flow (denoted *L*) takes place in the tubing above the first injection point and after a gas injection point if all gas dissolves in the liquid. Two-phase flow (designated as *TP*) appears below the gas injection valve, when NCGs is not complete dissolved at the central tubing below injection valves. Note also that, if bottom hole pressure is not high enough, the tubing cannot be filled with liquid up to the wellhead and liquid flashes into vapour on the top part of the tubing (previously defined "free fall" section). The pressure is then equal to the saturation vapour pressure; the liquid falls free downward on the wall of the tubing, whereas the vapour flows at the centre of the tubing. This type of flow (designated as *FF*) occurs above the free water level in the tubing. In the proposed reinjection approach, gas must be injected directly in the liquid phase to be dragged by liquid downwards to the reservoir and not accumulated in the "free fall" section.

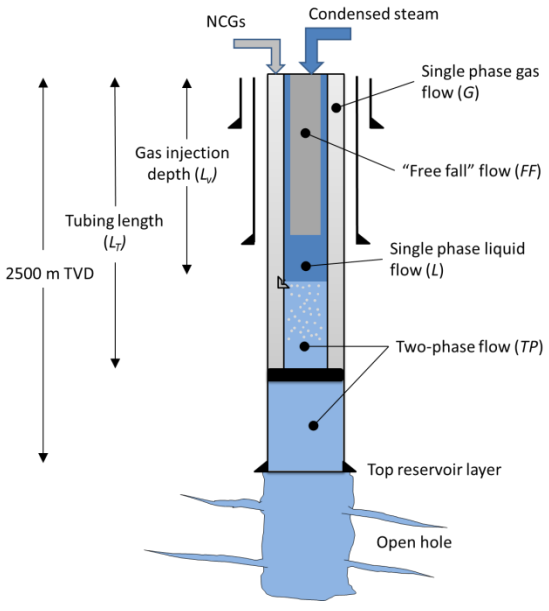

Figure 2: Well completion, abbreviations and design parameters; sensitivities to tubing length, L_T, gas injection depth, L_v, tubing inner diameter, D_T, and inter-point injection point distance, dL_v , were also assessed and are presented in the result section.

For two-phase flow, both phases can flow according to different flow patterns, which are determined by the interfacial structures between both phases. Flow regimes are known to vary with many factors, including the fluid properties, the flow channel size, geometry and orientation, body force field, injection method and flow rates. Downward two-phase flow regimes are usually classified into four or five categories (Julia et al., 2013) (Fig. 3a). When the gas phase is dispersed in the continuous liquid phase regardless the density and the size of the gas bubbles, the flow is named as dispersed flow (designated as *D*; bubbly and cap-bubbly on Fig. 3a). When the size of the gas bubbles approach that of the pipe diameter, the flow is denoted as intermittent (designated as

I; slug and churn-turbulent pattern on Fig. 3a). Finally, when the gas phase is flowing continuous at the core (with or without dispersed liquid droplets) and the liquid on the wall, the regime is called annular (designated as *A* on Fig. 3a). The different flow regimes are usually represented as a transition flow map in which the gas superficial velocity, U_G, is plotted against the superficial liquid velocity, U_L (Fig. 3b). The transition boundaries between the different patterns are given by solid lines. For a constant geometry, the transition between the different flow regimes can occur by modifying the velocity of the gas and/or the liquid.

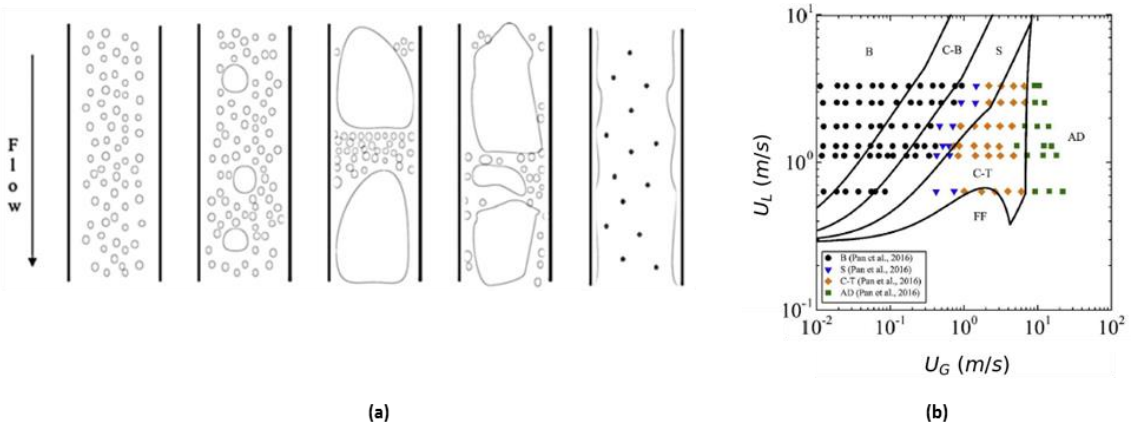

Figure 3:a) Two phase flow regimes (from left to right): bubbly, cap-bubbly, slug, churn-turbulent and annular (Julia et al., 2013) and b) flow map (Lokanathan and Hibiki, 2018).

The identification of the two phase flow regimes is important, as the gas flow structure affects strongly the dissolution rate of the gas into the liquid phase and the effective entrainment of the gas by the liquid phase. When the gas is in the form of small bubbles, dispersed in the continuous liquid fluid, the dissolution are enhanced by the high gas liquid contact surface. In addition, the bubbles may be easily drag downwards. The dispersed flow pattern is therefore the most favourable for the reinjection efficiency, while annular flow is the less desired.

Lokanathan and Hibiki (2016, 2018) created a database of experimental points (water-air systems, 1" to 4" diameter and up to 2 bar working pressure) and correlations available in the literature and proposed new criteria for all transitions. The transition criteria that are of interest in the current study are:

Dispersed to Intermittent: $\alpha \geq 0.175$ (1)

To Annular: $\alpha \geq 0.43$ (2)

where α is the void fraction, which is one of the most crucial two-phase parameter. Due to its significance, the void fraction has been measured experimentally and several models have been proposed. Among the models, those based on the drift flux model, originally proposed by Zuber and Findlay (1965), have been proven to be the most accurate. In the work of Lokanathan and Hibiki (2018), the drift-flux model developed by Goda et al. (2003), is selected to define the void fraction both for upward and downward flows.

Bhagwat and Ghajet (2014) perform a literature review and created an extensive database with experimental data covering a wide range of fluid combinations and working conditions, pipe diameters and orientations. Two separate sets of equations were proposed for drift flux model parameters namely, the distribution parameter and the drift velocity. These equations are defined as a function of several two phase flow variables and are system independent. However, the data used for vertical downward flow were very limited. Nevertheless, this model is considered in the study for the calculations of the void fraction and the drift flux velocity.

3.1.2 Pressure Drop Calculations

The total pressure drop is the sum of the losses due to the friction and gravity:

$$\left(\frac{dP}{dx}\right)_{k,S} = \left(\frac{dP}{dx}\right)_{k,f} + \left(\frac{dP}{dx}\right)_{k,g} \tag{3}$$

where the indices are $S = A, T$ for the annulus or the tubing space, $k = G, L, TP$ for the gas, liquid and two-phase flow, f refers to the friction losses and g to losses due to gravity. The gravity pressure drop is:

$$\left(\frac{dP}{dx}\right)_{k,g} = \left[\alpha\rho_G + (1-\alpha)\rho_L\right] g \sin\theta \tag{4}$$

where g the acceleration of gravity. For liquid phase flow $\alpha = 0$ and $\alpha = 1$ for gas flow, and the above equation will express the gravitational losses for single phase flows.

Yao et al. (2018) developed a model for predicting the pressure drop due to friction of gas-liquid flows in vertical tubes. It is a semi-empirical correlation that treats the two-phases as separated phases and it is based on the model proposed by Chisholm (1967) who improved the simplified Lockhart-Martinelli correlation. A parameter to consider the effect of buoyancy was introduced into

the separated flow model. They compared their model against experimental data for water-air flowing in vertical downward tubes with inner diameter up to 65 mm and with operational pressure up to 2.8 bar. The experimental data cover the entire flow map and the correlation is independent of the flow regime. For single phase flow, the pressure losses due to friction can be calculated by the well-known Darcy–Weisbach equation and the Darcy friction factor from the Colebrook equation (Stewart et al, 2001).

In the case of "free fall" region, the liquid water is assumed in thermodynamic equilibrium with its vapour at the local temperature and saturation pressure. In that case, the pressure drop should stay close zero meaning the losses due to friction are balanced by the gravitational pressure drop until the water interface is reached.

3.2 Thermal Modelling

The thermal modelling consists in calculating the heat transfer between the fluids, in the annulus and the central tubing space, and the surrounding bedrock system. Even though the heat transfer is multidimensional, it is assumed that it takes place only on the radial direction. Moreover, if two phases are present, it is assumed that the phase temperatures are equal meaning the residence time is sufficient to get homogenized temperature. For the study, the temperature profile in the surrounding rock has been assumed linear but any data from the geothermal temperature profile could be taken into account in the model.

The fluid enthalpy variation ΔH_t is due to the energy losses between the well completion and the surroundings, Q_l and the gravitational potential energy, Q_g:

$$\Delta H_t = Q_l + Q_g = Q_l + \rho_k U_k g \sin\theta \tag{5}$$

Two mechanisms of energy transfer considered: heat exchange between the solid materials (ground, cement and steel) due to the conduction and convection transfer due to the fluid motion in the annulus and the central tubing spaces. The concept of the thermal resistance, R_θ, is applied for developing the thermal model. For each material (ground, cement, steel, fluid), the heat exchange can be calculated by a characteristic physical property. In solid materials, the conductance transfer is expressed with the thermal conductivity, λ, of the material, whereas the convection with the convective heat transfer coefficient, h derived from Nusselt number correlations. Basically, the total resistance of the cross section is the sum of the thermal resistances of the successive material layers.

Two mechanisms of energy transfer considered: heat exchange between the solid materials (ground, cement and steel) due to the conduction and convection transfer due to the fluid motion in the annulus and the central tubing spaces. The concept of the thermal resistance, R_θ, is applied for developing the thermal model. For each material (ground, cement, steel, fluid), the heat exchange can be calculated by a characteristic physical property. In solid materials, the conductance transfer is expressed with the thermal conductivity, λ, of the material, whereas the convection with the convective heat transfer coefficient, h derived from Nusselt number correlations. Basically, the total resistance of the cross section is the sum of the thermal resistances of the successive material layers.

At the beginning of the injection process, the thermal inertia of the surrounding well area influences the injection fluid temperature profile as the gradient in the casing is high until the surrounding bedrock temperature stabilized and the temperature becomes relatively uniform (Pan et al, 2011). Bérest (2019) studied heat transfer in salt caverns and the wellbore thermal effect where the rock temperature does not equal to the injected fluid temperature. The rock temperature experiences significant changes in a cylinder whose radius can be assessed by $R_s = \sqrt{k_R\, t_0}$ where k_R is the thermal diffusivity of the bed rock. With ground thermal properties of the present study case, thermal conductivity of 1.73 W/m/K, density of 2563 kg/m^3 and heat capacity of 1046 J/kg/K, k_R is equal to 6.4 10^{-7} m^2/s. For t_0 equal to one week period, R_s reaches around 0.62 cm. (Bérest, 2019) compared the transient inertia of the cylinder rock defined by R_s to the heat amount of the gas flowing in the well and concluded that the change in rock temperature is much larger than the gas temperature change, and gas flow could be considered as adiabatic.

A simplified and complementary approach to assess thermal exchanges in the well consists in calculating the steady-state temperature profile of water injected in a tube at a given flow rate and exchanging heat with a bed rock at constant temperature. The characteristic radius R_s defines a distance where the temperature of the rock can be assumed constant during the fluid flow from the wellhead down to the bottom hole. Under these conditions, the temperature profile in the well can be calculated analytically as described by Eq. (6). For x equal to the well length L_w, the exponent of the equation is a dimensionless number representing the thermal diffusion rate in the bedrock divided by the thermal advection rate of the geothermal fluid in the injection well. For the present study case, its absolute value is around 2.6 10^{-2} meaning the advection is largely predominant and the fluid temperature evolution in the well is close to the adiabatic temperature profile.

$$\dot{m}_f Cp_f \frac{\partial T_{w,x}}{\partial x} = -\frac{\pi\, r_w \lambda_s}{R_s}\left(T_s - T_{w,x}\right) \Rightarrow T_w(x) - T_{w,x=0} = \left(T_s - T_{w,x=0}\right)\left[1 - \exp\left(-\frac{\pi\, r_w \lambda_s}{\dot{m}_f Cp_f R_s}\, x\right)\right] \tag{6}$$

where $\dot{m}_f$ and Cp_f are the mass flow rate and the heat capacity of the fluid flowing inside the well, $T_{w,x}$ is the fluid temperature along the well, T_s is the temperature at a distance R_s from the well, r_w the well radius and λ_s is the thermal conductivity of the surrounding ground.

3.3 Valve Modelling

Gas-lift is an artificial lift technique which has been widely applied in oil & gas production wells (Clegg et al., 1993), where high pressure gas is injected through the annulus into the production tubing to alleviate the fluid density and provide sufficient energy to produce the fluid. In the case of NCG reinjection, the valves operate similarly to oil and gas wells (Shafaei et al., 2012). To open valve, two conditions must be fulfilled: the annulus pressure to be higher than the central tubing pressure and the central tubing

pressure higher than a given threshold. The first criterion secures that only gas is injected in the desired direction (from annular to casing), while the second one ensures that gas is injected inside the liquid phase (or the "free-fall" section), below the water level.

The mass flow through the valve is assumed an isentropic compressible flow and the gas flow rate is related to the upstream stagnation pressure, P_A, and temperature, T_A, the static pressure just downstream of the valve, P_T, and a characteristic reference area of the valve, A_v. The real gas flow effects are included by means of a discharge coefficient, C_D. The mass flow rate through the valve, $\dot{m}_{G,V}$, that connects the annulus space to the central tubing allowing only gas to move can be calculated based on the below expression (Guo et al., 2017). If the ratio of the downstream and upstream pressure at the injection point is lower than $P_T/P_A < 0.52$, the flow is considered as choked flow and it is independent of the downstream pressure, P_A. This is not valid in the simulations that were performed since always was $P_T/P_A > 0.92$.

$$\dot{m}_{G,V} = \frac{C_D A_V P_A}{\sqrt{\frac{R}{M_W} T_A}} \left(\frac{P_T}{P_A}\right)^{\frac{1}{\gamma}} \sqrt{\frac{2\gamma}{\gamma+1}\left(1-\frac{P_T}{P_A}\right)} \tag{7}$$

where γ is the compressibility factor, M_w the molecular weight and R the gas constant (8.314 J/mol/°C).

3.4 Thermodynamic Data

Simple equations of state and correlations are used for calculating the physical and thermodynamic phase properties (density, viscosity, saturation pressure etc.) . Some properties (heat capacity, thermal conductivity etc.) were kept constant with pressure and temperature. For the dissolution for CO_2 in water, the tabulated data given by Duan and Sun (2003) are used for different pressures and temperatures. In a future step, a complete thermodynamic model (Di Lella and Mougin, 2020) and a kinetic model, similar to Blyton and Bryant (2013), for the dissolution of CO_2 will be integrated in the simulation tool.

3.5 Numerical Model

3.5.1 Space discretization

The well is uniformly discretized in space using the central difference scheme, as shown in Fig. 4. The length of each cell in all simulations is ΔL = 1 m and it is the same both in the annulus and the central space. All variables and properties, Φ, are calculated either on the cell edges or on the cell centres. Depending on the distance from the well head and the length of the tubing, the local geometry changes and a cell can contain the variables for the central tubing and the annulus. At the valve positions, dummy cells enable the mass and enthalpy transfers from the annular space to the central tubing with respect to the local pressure conditions.

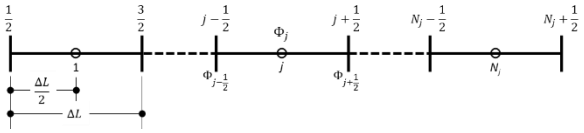

Figure 4: Well space discretization with the central scheme.

3.5.2 Boundary Conditions

Gas and water flow rates are imposed at the wellhead; also the reservoir pressure and the injectivity are given at all times. For high reservoir pressure, the modelling estimates the gas pressure at the compressor outlet and the water pressure at the pump outlet, whereas for low reservoir pressure, the gas pressure at the compressor and the height of the free fall at the top of the tubing are determined.

3.5.3 Discrete mass, momentum and enthalpy balances

The mass, *m*, conservations are written per component (*i*: water or CO_2) and per phase (gas, *G*, or liquid, *L*), whereas the pressure, *P*, equation and the enthalpy, *H*, balance are expressed for the overall flowing mixtures (single phase, two-phase and mixture). All balances are applied at the annulus, *A*, and the tubing, *T*, space and for the *j* cell (between *j*-½ and *j*+½ in the discretization scheme, excluding dummy cells with valves) are described by the below equations.

Gas mass balance per component in annular space: $\dot{m}_{G,i,A_{j+\frac{1}{2}}} = \dot{m}_{G,i,A_{j-\frac{1}{2}}} - \dot{m}_{G,i,V_j}$ (8)

Gas mass balance per component in the tubing: $\dot{m}_{G,i,T_{j+\frac{1}{2}}} = \dot{m}_{G,i,T_{j-\frac{1}{2}}} + \dot{m}_{G,i,V_j} - \dot{m}_{G,i,D_j}$ (9)

Liquid mass balance per component in the tubing: $\dot{m}_{L,i,T_{j+\frac{1}{2}}} = \dot{m}_{L,i,T_{j+\frac{1}{2}}} + \dot{m}_{G,i,D_j}$ (10)

Gas momentum balance in the annular space: $P_{A_{j+\frac{1}{2}}} = P_{A_{j-\frac{1}{2}}} - \left(\frac{dP}{dL}\right)_{G,A_j} \Delta L$ (11)

Overall momentum conservation in the tubing: $P_{T_{j+\frac{1}{2}}} = P_{T_{j-\frac{1}{2}}} - \left(\frac{dP}{dL}\right)_{k,T_j} \Delta L$ (12)

Gas enthalpy balance in the annular space: $H_{A_{j+\frac{1}{2}}} = H_{A_{j-\frac{1}{2}}} - \Delta H_{A_j} \Delta L$ (13)

Enthalpy balance in the tubing: $H_{T_{j+\frac{1}{2}}} = H_{T_{j-\frac{1}{2}}} - \Delta H_{T_j} \Delta L$ (14)

where $\dot{m}_{G,D}$ is the mass of CO_2 dissolved in the liquid in the central tubing.

3.5.4 Numerical resolution

The problem is solved using two iteration loops; an internal iteration loop on each cell to solve conservative equations and then propagating the results sequentially along the grid, and a global iteration loop for calculating, for fixed inlet conditions, the pressure at the outlet of the well. Two criteria have to be respected to stop the second iteration loop: 1) all gas injected in the annulus space has to flow to the central space through the gas-lift valves (gas mass conservation), and 2) the pressure at the outlet of the completion has to be consistent with the bottom hole pressure calculated from on the reservoir injectivity and pressure. The calculation module has been developed using Python 3.7.3.

4. RESULTS

4.1 Test case configuration

The depth of the well is 2500 m TVD (true vertical depth) and the internal diameter of the casing is 6 in. The total geothermal rate is 18 kg/s, 8% of which is NCGs (only CO_2 in the current study). The temperatures of the injected gas and liquid are 50 °C and 89 °C, respectively. The injected liquid is condensate steam; thus water with zero salinity. The reservoir pressure and temperature are 70 bar and 280 °C. Simulations performed for three different reservoir injectivity indexes: I = 0.7, 1.8 and 8.9 t/bar/h.

The main specificity of the selected test case is the low reservoir pressure, which results in an extended free fall zone at the top of the tubing while injecting water in the tube. The liquid column never reaches the wellhead with the studied injection conditions. As explained previously, the injected liquid flashes at the local temperature just after the wellhead valve. In the study case, the liquid pressure upstream the wellhead is always 10 bar (corresponding to the pressure of the stream coming from the last step of the process in the surface). and the injection temperature is 89 °C. Thus, the local pressure is equal to the water saturation pressure at 89 °C which is around 0.7 bar.

4.2 Only water injection

Before starting the injection of the gas on the well, only water is injected from the wellhead. Figure 5 shows the pressure profile in 3½ in inner diameter tubing when only liquid is being injected for the different injectivity indexes. The lower the injectivity, which corresponds to higher pressure at the bottom hole, the higher the water column. Since the injection of the gas should occur inside the liquid, it is obvious that at least one injection point should be below the depth of Fig. 5, depending on the injectivity.

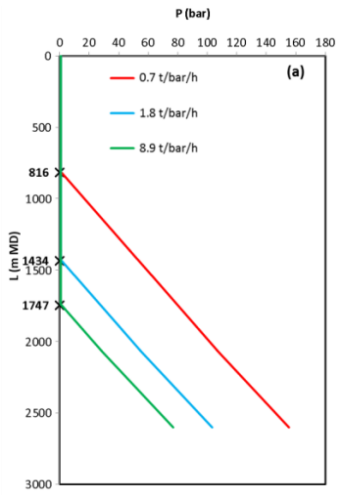

Figure 5: Pressure profiles along the central tube with no gas for different reservoir injectivity indexes.

4.3 Surface mixing

If gas and liquid are ideally mixed and injected on the surface, the demand on pumping and compression are not too high (Fig. 6a), especially for the high and moderate injectivity reservoirs. However, surface injection requires the well to be completely full of water before starting gas injection which is not the case as the liquid column never reaches the surface (Fig. 5). In order to succeed, it is necessary to start the injection by injecting gas deeper which requires higher gas compression or to use multiple injection points at different depths, as it will be shown later. Moreover, for the surface mixing, the intermittent flow pattern prevails in the entire length of the completion (yellow tubing section I on Fig. 6b), even annular flow regime appears in the vicinity of the well entrance for the higher injectivity (red tubing section A on Fig. 6b). Only, at the lower injectivity and in high depth, where the pressure and temperature are elevated and thus promoting the dissolution of the CO_2, dispersed bubbles may appear inside the continuous liquid phase (green tubing section D on Fig. 6b).

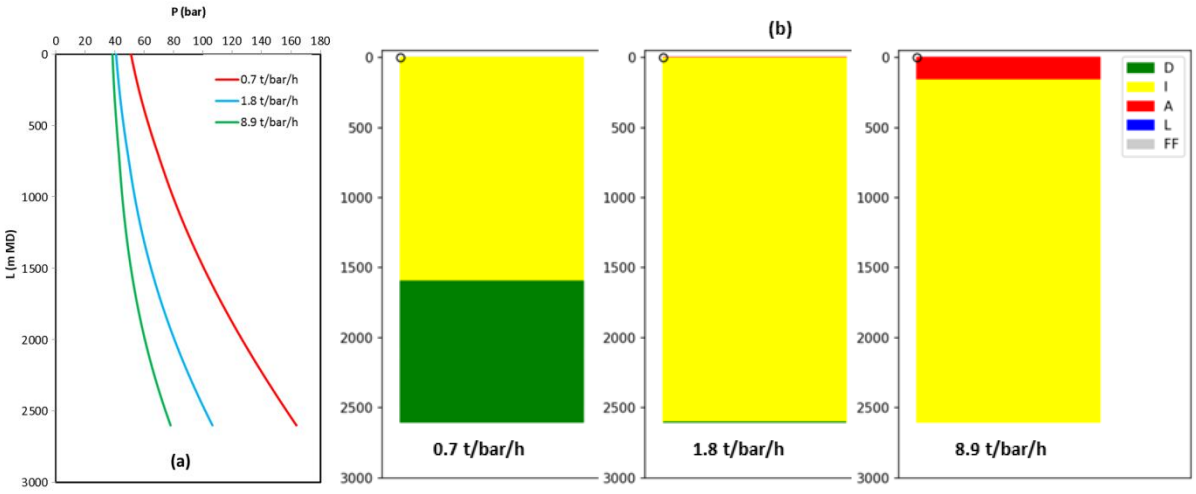

Figure 6: a) Pressure profiles and b) flow regimes along the well with gas and liquid mixing at the surface for the different reservoir injectivity indexes.

4.4 Sensitivity studies for the configuration with one injection point

Sensitivity studies were performed to optimise the length of the annulus space/length of the tubing, the inner diameter of the tubing and the position of the unique injection point. In all cases, the reservoir injectivity index was 1.8 t/bar/h and there was only one injection point at depth of 1490 m TVD. The opening area of the injection point is 1 in.

When injecting the gas from one point at depth below the water interface, the liquid column in the tube starts to raise (Fig. 7b). The longer is the tubing, more gas compression is needed at the surface and the water surface reaches higher position in the well. The liquid height above the injection point corresponds to a hydraulic head that should be overcome in order to inject gas; thus the higher is the liquid height above the injection point more gas pressure is required. However for the shorter tubing length of 1590 m, the risk of being in annular two-phase regime is higher. This can be seen by comparing the flow maps of Fig. 7c, where the part of the flow which is close to the transition line between the intermittent and the annular pattern shifts closer to the transition to dispersed flow for longer tubing. The longer tubing results in the restriction of the zone where the tubing inner diameter is wider (equal to the casing diameter) and as a consequence in the increase of the gas and the liquid superficial velocities. For operational and cost reasons, a 2000 m TVD long of the annulus space/length of the tubing is a good compromise.

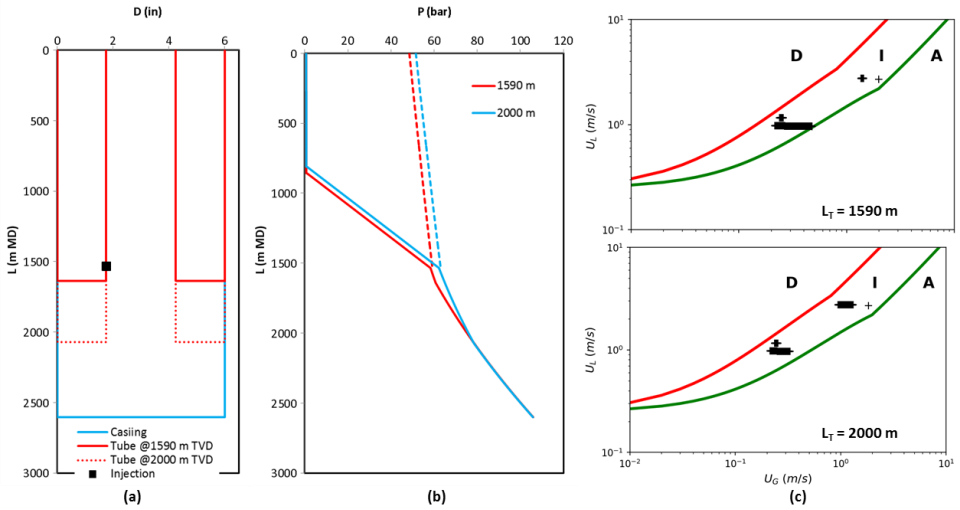

Figure 7: a) Well completion configuration, b) pressure profiles (dash line: gas profile in the annulus space, continuous line: liquid or two-phase profile in the tubing and casing space) and c) flow maps for injecting through 1 point for different length of the tubing space, L_T.

Figure 8 shows the results for different tube diameters with a tubing length equal to 2000 m TVD and with one injection point located at 1490 m TVD. For small diameter, the required pressure at the compressor outlet is higher with a shorter free fall section (Fig. 8b). However, the reduction on the inlet pressure is getting less pronounced for bigger tube diameters. Increase of the tubing inner diameter results in decrease of superficial gas velocity but the two-phase flow regime is always intermittent, whereas for the larger diameter approaches the annular transition (Fig.8). The diameter of 3.5 in was selected as the optimum diameter. A tubing with a 3 in internal diameter results in a high gas injection pressure (Fig. 8b), while a 4 in internal diameter results in a flow close to the Intermittent/Annular transition (Fig. 8c).

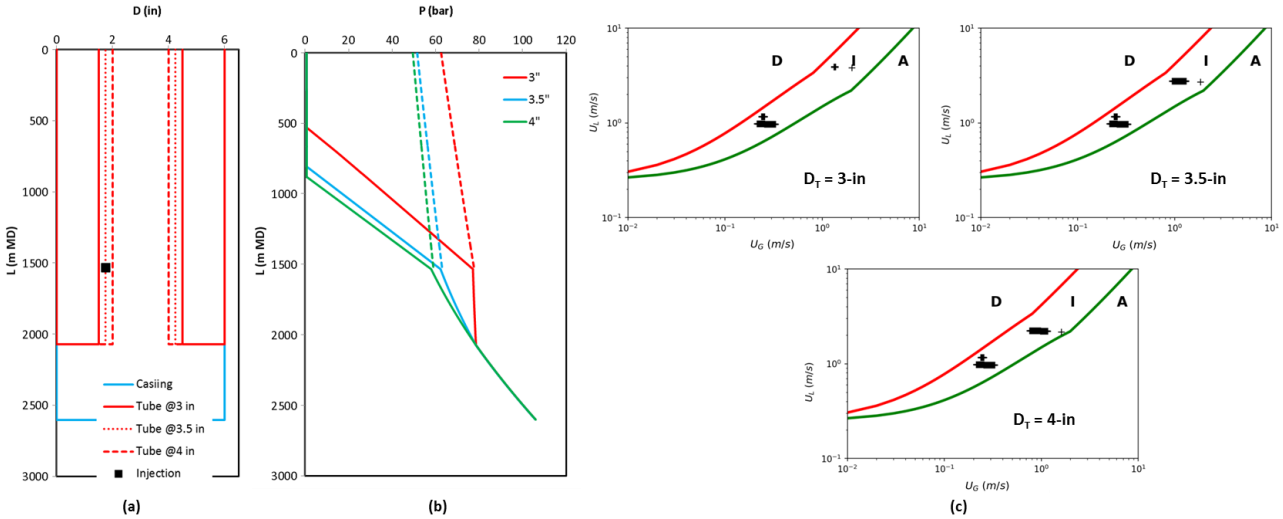

Figure 8: a) Well completion configuration, b) pressure profiles (dash line: gas profile in the annulus space, continuous line: liquid or two-phase profile in the tubing and casing space) and c) flow maps for injecting through 1 point for different tubing inner diameter, D_T.

As expected, the sensitivity to gas injection depth, L_v, shows that the deeper is the mixing point, more gas compression needed at the surface and deeper the water surface remained (Fig. 9a). For both cases, the two phase flow map across the tube is similar (Fig. 9b), with the intermittent pattern being well established.

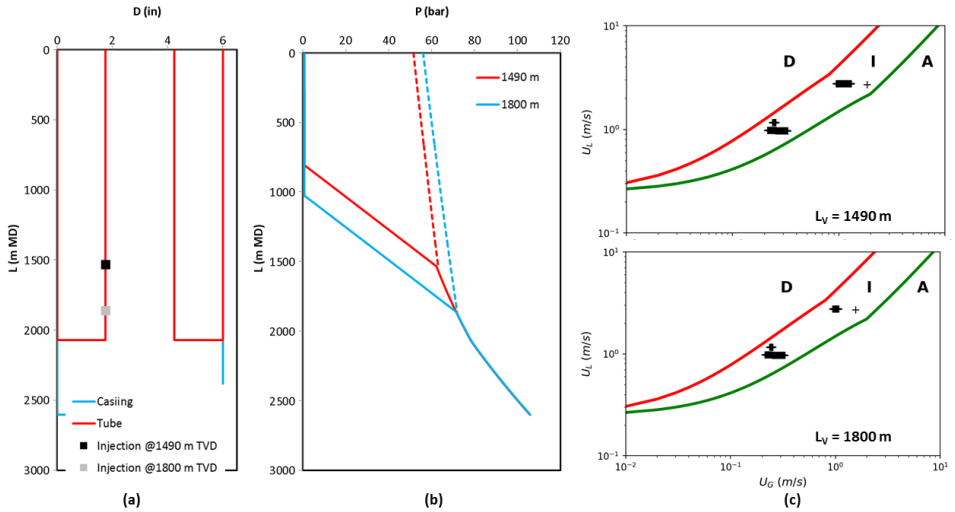

Figure 9: a) Well completion configuration, b) pressure profiles (dash line: gas profile in the annulus space, continuous line: liquid or two-phase profile in the tubing and casing space) and b) flow maps for injecting through 1 point for different gas injection depth, L_v.

4.5 Sensitivity studies with multiple injection points

Under steady state conditions, gas may be injected simultaneously through multiple injection points. Figure 10a shows the evolution of the pressure for different distance between the three consecutive injection points; the deeper valve is always at 1490 m TVD and the valves are located every 100 m, 200 m and 300 m. Despite the different distance, the pressure requirements at the surface are the same and the liquid level slightly increases with the distance. However, the two-phase flow maps are quite different (Fig. 10b). At smaller valve distance, the only-liquid region is broader, because injection takes place deeper where the pressure is higher and the injected CO_2 can be completely dissolved in the liquid phase. However, when all gas passes to the tube the regime is always intermittent.

Comparing with the case of injecting through one injection point (Fig. 7), the gas pressure at the wellhead is practically the same, but the liquid level at the tubing forced closer to surface. Operating in steady state conditions, the injection process through multiple injection points simultaneously does not have any pronounced advantage.

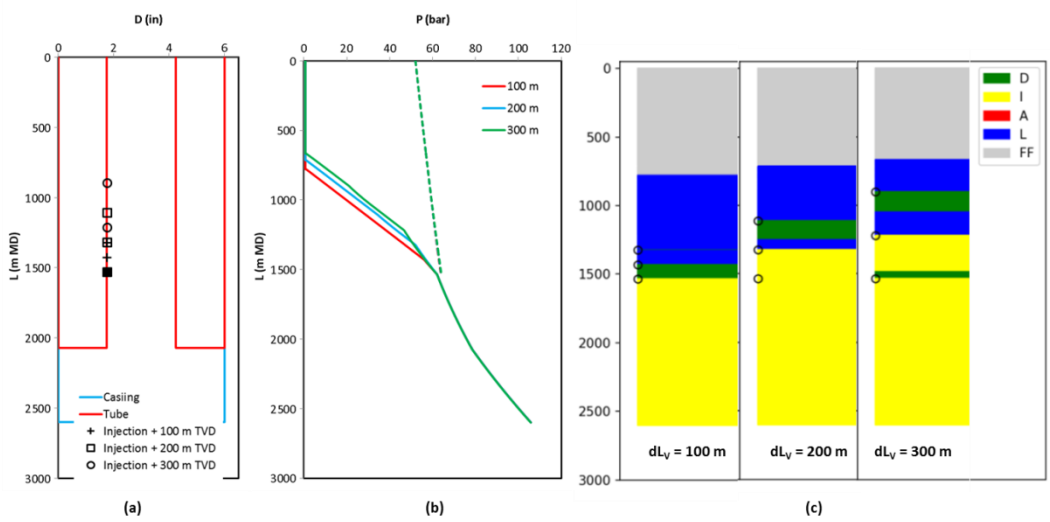

Figure 10: a) Well completion configuration, b) pressure profiles (dash line: gas profile in the annulus space, continuous line: liquid or two-phase profile in the tubing and casing space) and b) flow maps for injecting through 3 points for different points distance, dL_V.

4.6 Injection process start-up

Several injection points are used in order to facilitate and allow the start-up of the re-injection process. The procedure consists in starting to inject only water at the beginning for the water column to raise in the tubing, then to inject gas in the annular to increase the annular pressure and initiate the injection from the deeper point located in the water column. The water raises gradually with the amount of gas passing in the tubing and lightening the fluid column below the injection point. When the water column arrives at the level of the next injection point, its valve opens (only when the pressure in the tubing is higher than the threshold but lower than the pressure at the annulus at this depth) and all other valves become or remain close. Figure 11 presents such a case, for 3 valves at 1000, 1400 and 1800 m TVD.

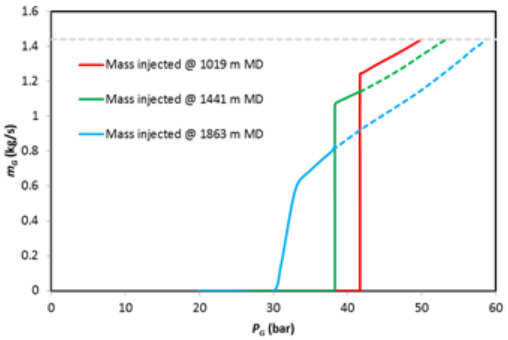

Figure 11: Start-up operation with three injection points for the medium reservoir injectivity (solid colour lines correspond to mass flow rate through the valves, dashed colour lines to mass flow rate if the specific valve kept open and others close, grey dash line to the gas injection rate target).

At the end of the start-up process, the well works under the steady state conditions and the required gas inlet pressure in this case is 14.5% lower than the compression using only the deepest injection point. The dash lines on the plot correspond to the case of continuing the injection only through one single point. The final pressure can be reduced further by designing additional injection points or by changing the distance between the valves so that the final injection takes place closer to the wellhead. Attention should be paid on the fact that, during this transient start-up procedure, not all gas can be injected in the reservoir, thus the redundant gas has to be vented temporary to the atmosphere or stored until the final steady state is reached.

After the start-up process the injection is under steady state conditions and occurs only through the point located at 1000 m TVD. The evolution of the liquid hold-up (fraction of liquid present in the tube cross section) along the depth is shown in Fig. 12 (left). In the vicinity of the well head, the injected liquid stream is being vaporized until it reaches the recompression region above the liquid column (437 m MD). The gas is being injected at 1019 m MD where the pressure in the tubing is above the valve threshold and below the annulus pressure. After this depth, the liquid hold-up changes because of the CO_2 dissolution in the water and the increasing local pressure.

Figure 12 (right) shows the steady state temperature profile in the well for the study case (x = 2500 m TVD, $T_{w,x=0}$ = 89 °C, $T_{s,x=2500}$ = 280 °C). After few meters from the wellhead, the gas temperature profile in the annulus space and the profile of the liquid/two-phase mixture in the central tubing/casing are practically equal and the two lines are overlapped until the injection point. Moreover, the flowing temperature slightly increase by 1°C from the inlet to the outlet of the well. It confirms the analysis done previously where flowing conditions in the well expect to be closed to adiabatic conditions.

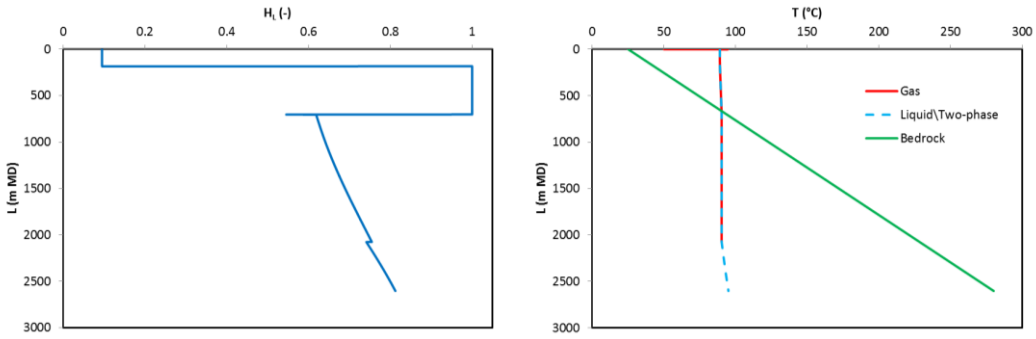

Figure 12: Liquid hold-up (left) and temperature (right) profiles under steady state operation and injection at 1000 m TVD (light grey line represents the injection point).

Generally, it was practically impossible to ensure a dispersed flow regime for all simulated cases according to chosen transition model. The initial amount of CO_2 with regard to the water quantity (2 mol CO_2/kg H_2O) combined with the conditions (pressure and temperature) in the entire length of the well results in the partial dissolution of the gas in the liquid. CO_2 content should be divided by a factor of two in order to dissolve all CO_2 at the same conditions. Thus, the velocity of the remaining gas quantity results in establishing the intermittent flow regime.

Comparing the above results with those of Stacey et al. (2016) reveals that the use of the proposed injection method with several injection valves and the gas being in the annulus space of the well string results in much lower injection pressure; for example mixing at a depth of 1200-1250 m TVD, the gas compression need is around 23% less (for a slightly lower total geothermal rate). In addition, by mixing the NGCs and water on the surface and injecting without using the inner tube string, the result showed on Fig. 7b agrees with that of Stacey et al. (2016).

5. CONCLUSIONS

A novel well completion design for the re-injection of both non-condensable gases and condensed water in the same well has been proposed. A 1D steady state model for simulating this process has been also developed to define the optimum reinjection configuration. Two components were considered in the injected fluids: NCG as pure CO_2 and the injected liquid pure H_2O. The advantages of injecting the gas through several points along the well string compared with injection at the well head after mixing the gas with the liquid or with injection through one point in relatively large depth have been demonstrated in the particular case of a low pressure reservoir. The required gas compression is weaker and the two-phase flow regime along the tubing is more favourable towards enhanced gas solubility, because of the shape and size of the gas bubbles inside the continuous liquid phase and gas entrainment. In addition, the injection through several points allows to secure the start-up procedures and adjusting well flow conditions based on effective reservoir injectivity. Using multiple injection points makes possible to raise the liquid column in wells for depleted reservoir and to inject directly the gas at lower pressure. Nevertheless, gas/liquid ratio has to be kept low enough to have efficient gas entrainment by the liquid. Further specific refinements are in progress to integrate thermodynamic calculations based on EoS and NCG dissolution kinetics. Moreover, the transient thermal inertia modelling of the well surrounding may be improved describing more accurately heat exchanges between the well and the rock mass especially at the early beginning of the injection.

ACKNOWLEDGMENTS

This project has received funding from the European Union's Horizon 2020 research and innovation programme under grant agreement No 818169.

REFERENCES

Aradottir, E.S.P., Gunnarsson, I, Sigfússon, B., Gunnarsson, G., Júliusson, B.M., Gunnlaugsson, E., Sigurdardóttir, H., Arnarsson, M.Th., and Sonnenthal, E.: Toward Cleaner Geothermal Energy Utilization: Capturing and Sequestering CO_2 and H_2S Emissions from Geothermal Power Plants, *Transport in Porous Media*, **108**, (2015), 61-84.

Benson, S., and Cole, D.R.: CO_2 Sequestration in Deep Sedimentary Formations, *Elements*, **4**, (2008), 325–331.

Bérest, P.: Heat transfer in salt caverns, *International Journal of Rock Mechanics and Mining Sciences*, **120**, (2019), 82-95.

Bhagwat, S.M., and Ghajar, A.J.: A Flow Pattern Independent Drift Flux Model Based Void Fraction Correlation for a Wide Range of Gas-Liquid Two-Phase Flow, *International Journal of Multiphase Flow*, **59**, (2014), 186-205.

Blyton, C.A., and Bryant, S.L.: Mass Transfer coefficient for CO_2 dissolution in brine, *Energy Procedia*, **37**, (2013), 4437-4444.

Burton, M., and Bryant, S.L.: Surface Dissolution: Minimizing Ground Water Impact and Leakage Risk Simultaneously, *Energy Procedia*, **1**, (2009), 3707–3714.

Chisholm, D.: A Theoretical Basis for the Lockhart-Martinelli Correlation for Two-Phase Flow, *Int J Heat Mass Tran*, 10, (1967), 1767-1778.

Clegg, J.D., Bucaram, S.M., and Hein, N.W.: Recommendations and Comparisons for Selecting Artificial-Lift Methods, *J Petrol Technol*, 45, (1993), 1128-1131.

Di Lella, A., and Mougin, P.: Thermodynamics of Geothermal fluids : A Benchmark Between Thermodynamic Models, from Henry's Approach to Advanced EoS (GECO Project), to be presented at World Geothermal Congress 2020, Reykjavik, IS (2020).

DiPippo, R.: Geothermal Power Generation: Development and Innovation, Cambridge, Woodhead publishing (2016).

Duan, Z., and Sun, R.: An Improved Model Calculating CO_2 Solubility in Pure Water and Aqueous NaCl Solutions from 273 to 533 K and from 0 to 2000 bar, *Chemical Geology*, **193**, (2003), 257-271.

Eke, P.E., Naylor, M., Haszeldine, S., and Curtis, A.: CO_2-Brine Surface Dissolution and Injection: CO_2 Storage Enhancement, *SPE Projects, Facilities & Construction*, **6**, (2011), 41-53.

Goda, H., Kim, S., Mi, Y., Finch, J.P., Ishii, M., and Uhle, J.,: Drift-Flux Model for Downward Two-Phase Flow, *International Journal of Heat and Mass Transfer*, **46**, (2003), 4835–4844.

Guo, B., Liu, X., and Tan, X.: Petroleum Production Engineering, Elsevier (2017).

Julia, J.E., Liu, Y., Hibiki, T., and Ishii, I.: Local Flow Regime Analysis in Vertical Co-Current Downward Two-Phase Flow, *Experimental Thermal and Fluid Science*, **44**, (2013), 345–355.

Koide, H., and Xue, Z.: Carbon Microbubbles Sequestration: A Novel Technology for Stable Underground Emplacement of Greenhouse Gases into Wide Variety of Saline Aquifers, Fractured Rocks and Tight Reservoirs, *Energy Procedia*, **1**, (2009), 3655-3662.

Lokanathan, M., and Hibiki, T.: Flow Regime, Void Fraction and Interfacial Area Transport and Characteristics of Co-Current Downward Two-Phase Flow, *Nuclear Engineering and Design*, **307**, (2016), 39-63.

Lokanathan, M., and Hibiki, T.: Flow Regime Transition Criteria for Co-Current Downward Two-Phase Flow, *Progress in Nuclear Energy*, **103**, (2018), 165-175.

Pan, L., Oldenburg, C.M., Pruess, K., and Wu, Y.S.: Transient CO_2 Leakage and Injection in Wellbore-Reservoir Systems for Geologic Carbon Sequestration, *Greenh Gases*, 1, (2011), 335-350.

Rathnaweera, T.D., Ranjith, P.G., Perera, M.S.A., and Haque, A.: Influence of CO_2−Brine Co-injection on CO_2 Storage Capacity Enhancement in Deep Saline Aquifers: An Experimental Study on Hawkesbury Sandstone Formation, *Energy Fuels*, **30**, (2016), 4229−4243.

Shafaei, M.J., Abedi, J., Hassanzadeh, H., and Chen, Z.: Reverse Gas-Lift Technology for CO_2 Storage into Deep Saline Aquifers, *Energy*, **45**, (2012), 840-849.

Shariatipour, S.M., Mackay, E.J., and Pickup, G.E.: An Engineering Solution for CO_2 Injection in Saline Aquifers, *International Journal of Greenhouse Gas Control*, **53**, (2016), 98-105.

Sigfusson, B., Gislason, S.R., Matter, J.M., Stute, M., Gunnlaugsson, E., Gunnarsson, I., Aradottir, E.S., Sigurdardottir, H., Mesfin, K., and Alfredsson, H.A., Wolff-Boenisch, D., Arnarsson, M.Th., and Oelkers, E.H.: Solving the Carbon-Dioxide Buoyancy Challenge: The design and Field Testing of a Dissolved CO_2 Injection System, *International Journal of Greenhouse Gas Control*, **37**, (2015), 213-219.

Stacey, R.W., Norris, L., and Lisi, S.: OLGA Modeling Results for Single Well Reinjection of Non-Condensable Gases (NCGs) and Water, *GRC Transactions*, **40**, (2016), 931-939.

Stewart, W.E., Bird, R.B., and Lightfoot, E.N.: Transport Phenomena, New York, J. Wiley (2001).

Suzukia, K., Miida, H., Wada, H., Horikawa, S., Ebi, T., and Ina, K.: Feasibility Study on CO_2 Micro-Bubble Storage (CMS), *Energy Procedia*, **37**, (2013), 6002-6009.

Yao, C., Li, H., Xue, Y., Liu, X., and Hao, G.: Investigation on the Frictional Pressure Drop of Gas Liquid Two-phase Flows in Vertical Downward Tubes, *International Communications in Heat and Mass Transfer*, **91**, (2018), 138-149.

Zendehboudi, S., Khan, A., Carlisle, S., and Leonenko, Y.: Ex Situ Dissolution of CO_2: A New Engineering Methodology Based on Mass-Transfer Perspective for Enhancement of CO2 Sequestration, *Energy Fuels*, **25**, (2011), 3323–3333.

Zendehboudi, S., Shafiei, A., Bahadori, A., Leonenko, Y., and Chatzis, I.: Droplets Evolution During Ex Situ Dissolution Technique for Geological CO_2 Sequestration: Experimental and Mathematical Modelling, *International Journal of Greenhouse Gas Control*, **13**, (2013), 201–214.

Zirrahi, M., Hassanzadeh, H., and Abedi, J.: The Laboratory Testing and Scale-Up of a Downhole Device for CO_2 Dissolution Acceleration, *International Journal of Greenhouse Gas Control*, **16**, (2013), 41–49.

Zuber, N. and Findlay, J.: Average Volume Concentration in Two Phase Systems, *ASME Journal of Heat Transfer*, **87**, (1965), 453–468.